Engineering Geology 103 (2009) 127–133

Contents lists available at ScienceDirect

Engineering Geology

journal homepage: www.elsevier.com/locate/enggeo

CAT-scan analysis of sedimentary sequences: An ultrahigh-resolution paleoclimatic tool

Guillaume St-Onge [a,b,*], Bernard F. Long [c,b]

[a] Institut des sciences de la mer de Rimouski (ISMER), Université du Québec à Rimouski, 310 allée des Ursulines, Rimouski, Canada G5L 3A1
[b] GEOTOP Research Centre, P.O. Box 8888, Succ. Centre-ville, Montréal, Québec, Canada H3C 3P8
[c] Institut national de la recherche scientifique Centre Eau, Terre et Environnement, 490 rue de la couronne, Québec, Québec, Canada G1K 9A9

ARTICLE INFO

Article history:
Accepted 3 June 2008
Available online 20 July 2008

Keywords:
CAT-scan
Sediments
Climatic oscillations
Postglacial
Glaciomarine
Holocene
Sangamonian
St. Lawrence Estuary

ABSTRACT

Paleoclimate research is essential to determine the natural variability of climate and to place the current climate change into its natural context. The current need is to generate the highest temporal resolution paleoclimatic reconstructions possible in order to assess the natural variability of the climate system, but also to test the ability of numerical models to simulate conditions different from the ones observed with the relatively short instrumental records. In this paper, we show that CAT-scan analysis of sedimentary sequences, with its 1 mm downcore resolution, can be used to identify millennial to seasonal cycles in sedimentary sequences. In examples from the St. Lawrence Estuary, Eastern Canada, spectral analysis of the CAT-scan data from Holocene postglacial sediments revealed millennial- to centennial-scale oscillations possibly associated with either solar variability, changes in relative sea-level or tidal amplitude. Similarly, spectral analysis of Holocene and Sangamonian glaciomarine sequences revealed decadal- to annual-scale oscillations with periods close to the one previously associated with the North Atlantic Oscillation (NAO), whereas spectral analysis of the CAT-scan data from the Sangamonian rhythmites possibly revealed seasonal cycles.

1. Introduction

Paleoclimate research is essential to determine the natural variability of climate and to place the current climate change into its natural context. The current need is to generate the highest temporal resolution paleoclimatic reconstructions possible in order to determine the natural variability of the climate system, but also to test the ability of numerical models to simulate conditions different from the ones observed with the relatively short instrumental records. Paleoclimatic reconstructions with an annual to decadal resolution are now emerging from tree-ring ring (e.g., D'Arrigo et al., 2003; Gray et al., 2004) and ice-core chronologies (Appenzeller et al., 1998; Stenni et al., 2003; Vinther et al., 2003), corals (Felis et al., 2000; Cobb et al., 2003), varved lacustrine sediments (Pepper et al., 2004; Prasad et al., 2004) and speleothems (Frisia et al., 2003; Lachniet et al., 2004; Tan et al., 2004). Unfortunately, these types of records are not ubiquitous throughout the world and their analysis rather time consuming with traditional methods.

On the other hand, computerized axial tomography (CAT-scan) allows the rapid visualization of both longitudinal and traversal sections of sedimentary cores. This non-destructive and very high-resolution method (~0.1 to 1 mm) has been previously used to identify sedimentary structures (Holler and Kögler 1990; Orsi et al., 1994), to determine the mode of sediment deposition (Crémer et al., 2002), to characterize the benthic community (Mermillod-Blondin et al., 2003; Michaud et al., 2003), to establish a high-resolution stratigraphy (Boespflug et al., 1995) and to evaluate the physical properties of sediments (Wellington and Vinegar 1987; Kantzas et al., 1992; Orsi et al., 1994; Amos et al., 1996). In this paper, we will show how CAT-scan analysis can be applied to sedimentary sequences to generate a continuous ultrahigh-resolution paleoclimatic tool that can be used to identify millennial- to seasonal-scale climatic oscillations.

2. Geological setting

In this paper, we will present examples from three sedimentary sequences sampled in the St. Lawrence Estuary, Eastern Canada (Fig. 1). Previous work based on high-resolution seismo-stratigraphy and piston cores has defined the tills, glaciomarine sediments and postglacial muds that comprise the regional stratigraphy of the area for the Late Pleistocene to Holocene (Syvitski and Praeg, 1989; Josenhans and Lehman, 1999). In addition, a detailed sedimentological and palynological record drilled on shore at the Île-aux-Coudres (Occhietti et al., 1995), in the middle estuary of the St. Lawrence Estuary, revealed the presence of glacial Illinoian and interglacial Sangamonian sediments (marine isotopic stage 6 to 5e, 130–80 kyr). In recent sediments, fine

* Corresponding author. Institut des sciences de la mer de Rimouski (ISMER), Université du Québec à Rimouski, 310 allée des Ursulines, Rimouski, Canada G5L 3A1. Tel.: +1 418 723 1986x1741; fax: +1 418 724 1842.
E-mail address: guillaume_st-onge@uqar.qc.ca (G. St-Onge).

0013-7952/$ – see front matter © 2008 Elsevier B.V. All rights reserved.
doi:10.1016/j.enggeo.2008.06.016

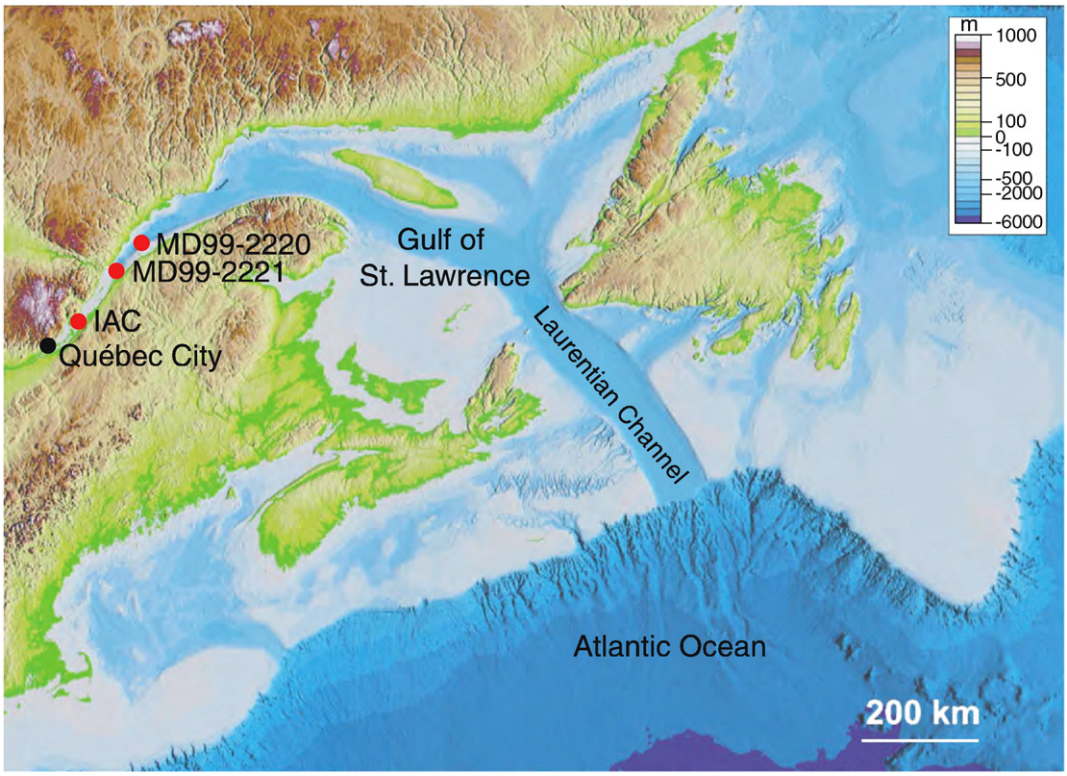

Fig. 1. Location of the sampling sites of cores 2220, 2221 and IAC in the St. Lawrence Estuary, Eastern Canada. Modified from Shaw et al. (2002).

grained, greenish-grey muds are observed on the deep central parts of the Laurentian Channel, whereas sandy muds are present on the sides and lower slopes as well as on the headward parts of the Laurentian Channel (Loring and Nota, 1973).

3. Materials

In the Lower St. Lawrence Estuary (Fig. 1), Calypso piston cores MD99-2220 (48°38.32′N/68°37.97′W, water depth: 320 m, length: 51.6 m) and MD99-2221 (48°10.60′N/69°30.35′W, water depth: 212 m, length: 31.0 m) were raised from the Laurentian Channel, a long U-shaped glaciated valley with depths between 200 and 540 m, during the 1999 IMAGES-V (International Marine Past Global Change Study) oceanographic campaign on board the RV *Marion Dufresne II*. In the Middle Estuary, core IAC was collected on shore in Île-aux-Coudres (Fig. 1).

4. Stratigraphy

4.1. Basic stratigraphy of cores MD99-2220 and MD99-2221

Detailed visual description of the cores MD99-2220 and MD99-2221 (hereinafter referred to as cores 2220 and 2221) along with the rock-magnetic and mean grain size data allowed the identification of two lithologic units (see St-Onge et al., 2003 for details). Unit 1 consists of grey to dark grey laminated to massive clays and is observed from the base to 1497 cm in core 2220 and from the base to 1353 cm in core 2221. Unit 2 is composed of dark grey bioturbated silty clays and dark grey bioturbated sandy mud in cores 2220 and 2221, respectively, and is observed from 1497 cm to the top of core 2220 and from 1353 cm to the top of core 2221. The transition from Unit 1 to Unit 2 is marked by a major change of the sedimentation rates, from >33 m/ka to ~1.5 m/ka, and reflects the drastic transition from glaciomarine to postglacial environments (St-Onge et al., 2003). This transition is notably clearly visible on the CAT-scan image of core 2221 (see Fig. 5 for example).

Using thirteen AMS ^{14}C dates on mollusc shells and paleomagnetic correlations with a nearby piston core, St-Onge et al. (2003) established a chronology for core 2220 over the last ~8500 cal BP, with sedimentation rates varying from 0.15 to 0.42 cm/year. Using the available ^{14}C dates from the glaciomarine sediments (St-Onge et al., 2003), we now extend this chronology to the base of the core (Fig. 2). The whole sequence now covers the last ~9400 cal BP.

4.2. Basic stratigraphy of core IAC

Core IAC is a 155-m long core that mainly corresponds to the transition from glacial Illinoian sediments to interglacial Sangamonian sediments. The first 58 m are composed of unconsolidated sediments while an unconsolidated to consolidated transition zone is observed between 58 and 79 m. Sediments are completely consolidated from 79 to 150 m. The core log presents the passage of ice-proximal deposits to deltaic regressive successions overlain by a thin veneer of Holocene material (Occhietti et al., 1995). In this paper, we will show examples from samples U5, U6 and U7, centered at 102 m, and lying within the centimeter-scale rhythmite succession of early Sangamonian age. This succession is interpreted to have been deposited in a glaciomarine environment similar to the one observed in cores 2220 and 2221 during the last deglaciation, with sedimentation rates in the order of 35 m/ka (Occhietti et al., 1995).

5. Methods

5.1. General principles

The CAT-scan uses a pixel intensity scale to quantify and map X-ray attenuation coefficients of the analyzed object on longitudinal (topograms) or transversal (tomograms) images. The resulting images are displayed on a grey scale, darker and lighter zones representing lower and higher X-ray attenuation, respectively. Grey scale values are

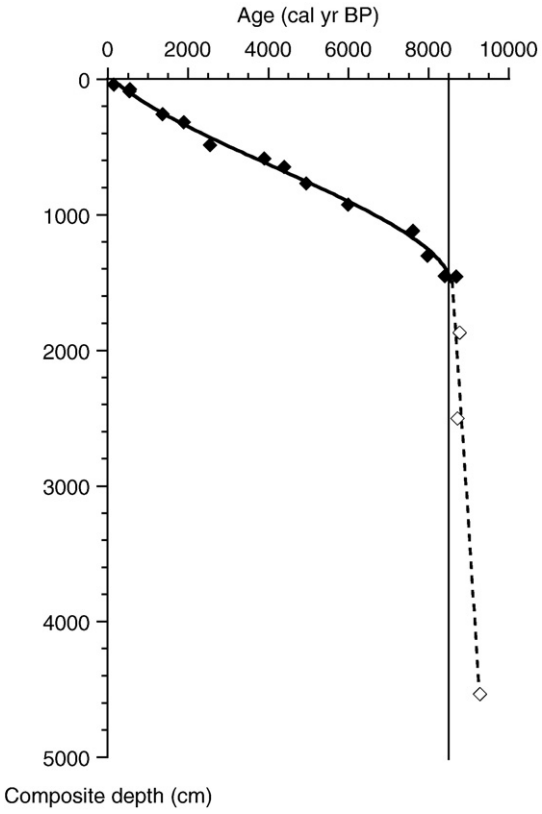

Fig. 2. New composite age model for cores 2220 and 2221. Depths of the dated material from core 2221 were transferred on core 2220 using the rock-magnetic, inclination and declination correlations (see St-Onge et al., 2003 for details). A third order polynomial fit was applied in the postglacial sediments, whereas a linear fit was used in the glaciomarine sediments to construct the final age model. The black vertical line illustrates the sharp change in sedimentation rates at the transition between glaciomarine and postglacial sediments.

expressed as CT numbers or Hounsfield units, obtained by comparing the attenuation coefficient (μ) to that of water (μ_w):

$$\mathrm{CT\,(Hounsfield\,Units)} = (\mu/\mu_w - 1) \times 1000 \quad (1)$$

A CT number is a complex unit related to the bulk density of the sediment, mineralogy, but also to the porosity (e.g., Boespflug et al., 1995; Crémer et al., 2002).

5.2. CAT-scan analysis of cores MD99-2220 and MD99-2221

CAT-scan analysis of the two Calypso cores was performed on 1.5 m core sections using a medical GE 7590 K Hi-speed Advantage 2.X CT/i CAT-scanner at the *Centre Hospitalier Régional de Rimouski*, Québec, Canada in 1999. Longitudinal images were obtained using a source radiation of 120 keV and 45 mA. The beam thickness was 1.5 mm. These images illustrate the average of the integration of the linear attenuation coefficients over the total thickness of the scanned object (the core diameter: ~11.5 cm) expressed in a plane view. Each longitudinal image has a dimension of 512×296 pixels, corresponding to a pixel resolution of 1.015 mm. For each core section, 5 images of 300 mm in length were thus acquired. A continuous image of both Calypso cores was then constructed using the Igor™ software by creating a matrix for each image and by incorporating each image matrix into each core final matrix. Using the same software, a continuous profile of the mean pixel intensity (CT number) on a width of 20 pixels (~2 cm) was then extracted from the newly constructed image. An artefact associated with the examination table is apparent on the first image of each core section and was only partially sampled by our procedure (Fig. 3). Erroneous CT numbers associated with this artefact were deleted from the continuous profile (Fig. 3). Because the images were obtained in a clean hospital environment, the end-caps of the different sections could not be removed and generated another artefact, which slightly increased the CT numbers. We corrected each core section for this small offset by visually adjusting the CT number profiles (Fig. 3). Because of the CAT-scan medical software limitations, the CT numbers obtained on the longitudinal images are not Hounsfield Units (HU). A first-order empirical relationship between the CT numbers of the longitudinal and transversal images (which are in HU) at a common depth, was thus determined (Cagnat, 2004) for both Calypso cores and is expressed below:

$$\mathrm{CT_L} = 195\ \mathrm{Ln}\ \mathrm{CT_T} - 1194, \quad r^2 = 0.85 \quad (2)$$

where CT_L is the CT number extracted from the longitudinal images and CT_T the CT number, in HU, extracted from the transverse image.

The relationship was then applied to the newly constructed longitudinal profile of both cores to convert the CT numbers in Hounsfield Units. Finally, to remove some of the noise induced by the very high sampling resolution (1.015 mm), a 11-point running average was applied to both cores CT number profiles.

5.3. CAT-scan analysis of core IAC

CAT-scan analysis of core IAC was realized on 0.9 m core sections using a medical GE 9800 third generation CAT-scanner at the *Centre Hospitalier Régional de Rimouski*, Québec, Canada in 1992. Longitudinal images were obtained using a source radiation of 120 keV and 100 mA. The beam thickness was 1.5 mm. Again, these images illustrate the average of the integration of the linear attenuation coefficients over the total thickness of the scanned object (the core diameter: ~9 cm) expressed in a plane view. Each longitudinal image has a dimension of 512×700 pixels, corresponding to a pixel resolution of 0.69 mm. For

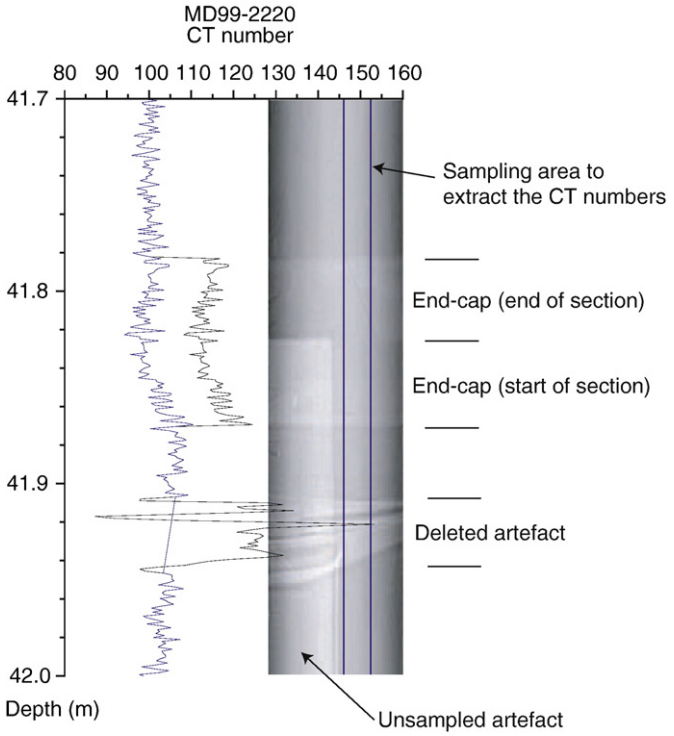

Fig. 3. Examples of artefacts introduced by the examination table and the end-caps along with the uncorrected (black) and corrected (blue) extracted CT numbers for cores 2220 and 2221. The blue area on the image represents the sampling area used to extract the CT numbers (20 pixels in width or ~2 cm). (For interpretation of the references to color in this figure legend, the reader is referred to the web version of this article.)

each core section, 2 images were thus acquired. As opposed to cores 2220 and 2221, where a continuous image for each core was constructed, a continuous image of each core section was only constructed for core IAC. Using an in-house program, a continuous profile of the mean pixel intensity (CT number) on a width of 10 pixels (~7 cm) was then extracted from selected core sections in the center of the images. Finally, as opposed to the more recent CAT-scan used for cores 2220 and 2221, the CT numbers obtained from the longitudinal images were directly in Hounsfield Units.

6. The CT number profile as an ultrahigh-resolution paleoclimatic proxy

The CT profiles of cores 2220 and 2221 are illustrated in Fig. 4 and compared to bulk density profiles measured on board the RV *Marion Dufresne II* using a GEOTEK Multi Sensor Core Logger (MSCL) at 2 cm intervals. The overall good agreement between the density and CT number profiles (r=0.9 for core 2220 and r=0.8 for core 2221) indicates that the CT number profiles primarily reflect changes in bulk density and can therefore be used as an ultrahigh-resolution proxy (resolution of 1.015 mm) of sedimentological changes. A logarithmic fit (upper red curves) and a linear trend (lower red curves) to the CT number data are also illustrated and probably reflect the influence of sediment consolidation on the sediment porosity and hence on the CT numbers. In addition, the CAT-scan image along with the derived CT number profile of core 2221 clearly highlights the drastic transition between the glaciomarine and postglacial sediments (Fig. 5).

In order to identify any climatic oscillations that may have been recorded in the CT number profiles, we performed spectral analysis on the Holocene postglacial and glaciomarine sediments of cores 2220, as well as on the Sangamonian glaciomarine sediments of core IAC. Prior to analysis, a cubic tendancy and the long-term trends associated with sediment consolidation were removed from the CT number profiles of cores IAC and 2220, respectively.

6.1. Millennial to secular climatic oscillations

Figs. 6 illustrates the spectral analysis results for the postglacial sediments of core 2220. Significant power is observed at periods of ~400 and ~1000 years. Some power close to the significant level is also observed at ~200 years. These periods are, for example, similar to periods (220, 480 and 940 years) identified in submerged sea grass from nearshore of the Baltic Sea (Yu, 2003) and in an Alaskan biogenic silica lacustrine record (195, 435 and 950 years; Hu et al., 2003). Periods between 200–300 were previously reported and associated with changes in solar activity (Stuiver and Braziunas, 1993a,b; Yu and Ito, 1999; Yu, 2003; Hu et al., 2003; Schimmelmann et al., 2003 and references therein), relative sea-level (Aaby, 1976; Kunzendorf and Larsen, 2002) and/or tidal amplitude (Yu, 2003). In addition, periods close to ~400 years were previously ascribed to solar variability (Yu and Ito, 1999 and references therein), whereas periods of 550 and 480 years were associated with changes in North Atlantic Deep Water circulation (Chapman and Shackleton, 2000) and/or changes in tidal amplitude (Yu, 2003), respectively. Similarly, 1000–1100-year cycles were previously associated with changes in thermohaline circulation (Stuiver et al., 1995; Chapman and Shackleton, 2000; Langdon et al., 2003) or relative sea-level (Fairbridge and Hillaire-Marcel, 1977; Rampino and Sanders, 1981). Unfortunately, the identification of

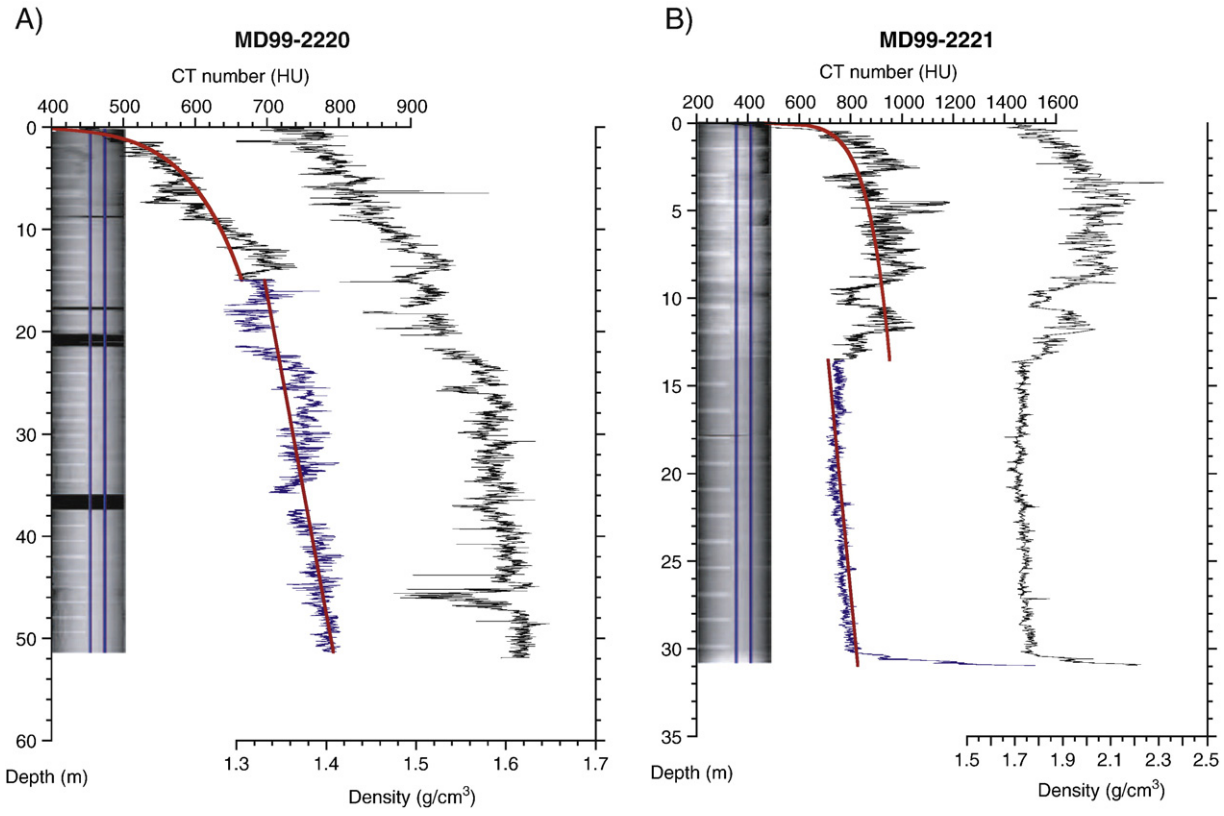

Fig. 4. Longitudinal CAT-scan image and corrected extracted CT number profiles of cores A) 2220 and B) 2221 compared with bulk density measurements obtained on board the *Marion Dufresne II* with a GEOTEK Multi Sensor Core Logger (MSCL) at 2 cm intervals. Postglacial sediments are in black, whereas the glaciomarine sediments are in blue. A 11-point running average was applied to both cores CT number profiles. A logarithmic fit (upper red curve) and a linear trend (lower red curve) probably associated with sediment consolidation are also illustrated. A sandy layer at the base of core 2221 was excluded from the linear fit. The blue area on the image of both cores represents the sampling area used to extract the CT numbers (20 pixels in width or ~2 cm). (For interpretation of the references to color in this figure legend, the reader is referred to the web version of this article.)

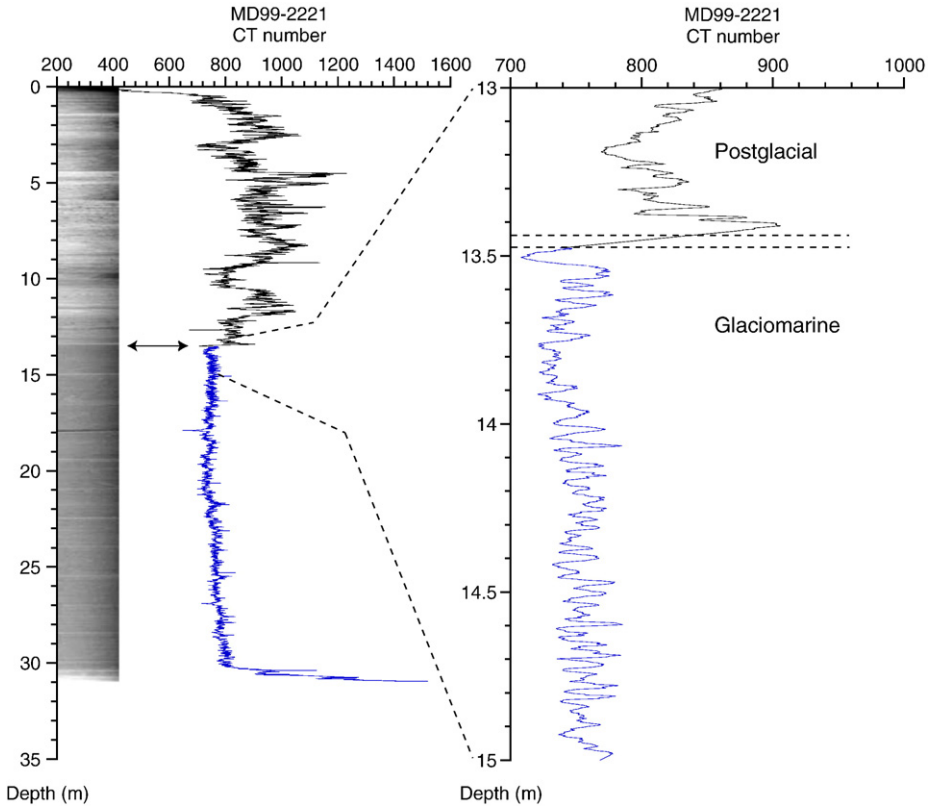

Fig. 5. Glaciomarine to postglacial transition. The left image illustrates the CAT-scan image and derived CT number profile of core 2221, whereas a zoom at the drastic transition from glaciomarine (lower blue curve) to postglacial (upper black curve) sediments is illustrated on the right. (For interpretation of the references to color in this figure legend, the reader is referred to the web version of this article.)

multiple periods with several possible causes indicate that further analyses are required to pinpoint the exact mechanism responsible for the CT number millennial- to centennial-scale variations. Nevertheless, the CAT-scan and following spectral analysis successfully allow the rapid identification of cyclic variations that are most likely associated with changes in the sediment bulk density.

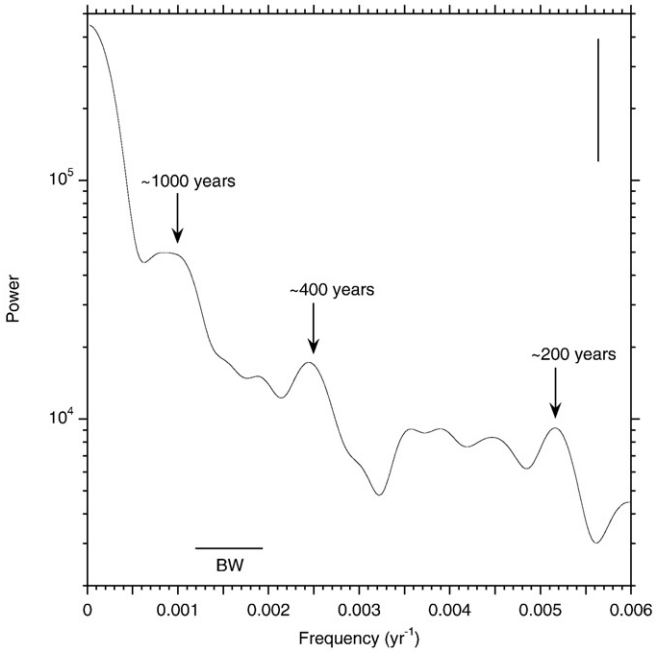

Fig. 6. Spectral analysis of core 2220 postglacial sediments (~0–8500 cal BP). The power spectrum was calculated with the Blackman–Tuckey method with a Bartlett window using the Analyseries 1.6 software (Paillard et al., 1996). Prior to analysis, the long-term logarithmic trend possibly associated with sediment consolidation was removed and the data were smoothed using a 11-point running average. The vertical and horizontal bars represent the 80% confidence level. BW = Bandwidth.

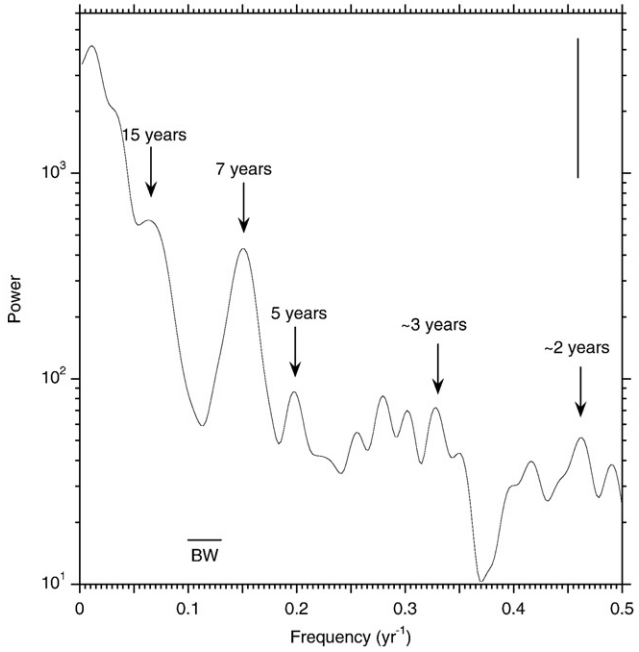

Fig. 7. Spectral analysis of core 2220 glaciomarine sediments from ~8600–8710 cal BP. The power spectrum was calculated with the Blackman–Tuckey method with a Bartlett window using the Analyseries 1.6 software (Paillard et al., 1996). Prior to analysis, the long-term linear trend probably associated with sediment consolidation was removed. The vertical and horizontal bars represent the 80% confidence level. BW = Bandwidth.

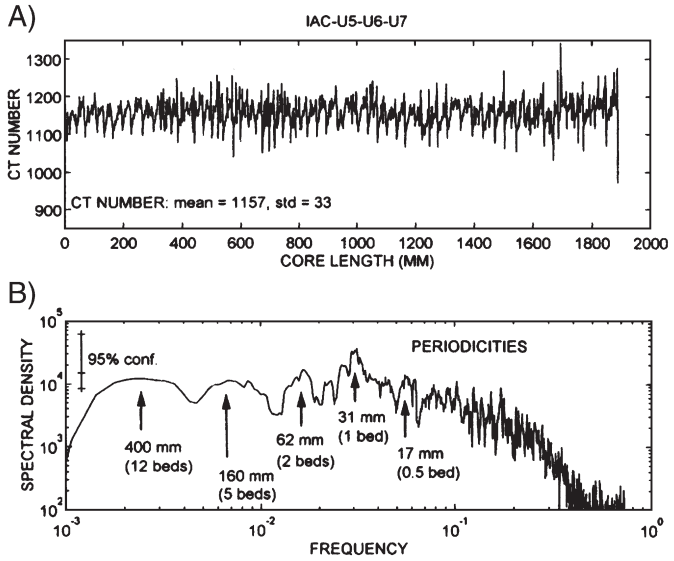

Fig. 8. A) CT number profile and B) spectral analysis of samples U6, U7 and U8 from core IAC Sangamonian glaciomarine sediments. The spectral analysis was performed with the Blackman–Tuckey method. Prior to spectral analysis, a cubic tendency was removed. Results are displayed after filtering the spectrum with a moving 7-point average (see Boespflug et al., 1995 for details). From Boespflug et al. (1995).

6.2. Decadal to annual climatic oscillations

Fig. 7 illustrates the power spectrum of the CT number profile from the glaciomarine sediments of core 2220 from ~8600–8710 cal BP. Significant power is observed at periods around ~2, 3, 7 and 15 years. Similar cycles of 2–3 years (Cook, 2003), 5–7 years (Schöne et al., 2004), 7–25 years (Cook, 2003) were previously identified in instrumental and proxy timeseries and associated with the North Atlantic Oscillation (NAO). Under present climatic conditions, the NAO is now recognized as the most prominent and recurrent pattern of winter atmospheric variability over the middle and high latitudes of the Northern Hemisphere, affecting both precipitations and temperatures (Hurrel et al., 2003). The similarity of the periods found in the CT number profiles of core 2220 with the ones associated with the NAO may imply a relationship between the latter and the sediments of core 2220. Such a link was also suggested for box-cored sediments sampled at the same site as core 2220 (St-Onge, 2004).

6.3. Annual to seasonal climatic oscillations

Fig. 8 illustrates the CT number profile and spectral analysis results for samples U5, U6 and U7 from core IAC. Apart from the annual cycle identified both visually (Occhietti et al., 1995) and with these spectral results (31 mm), significant power is observed at 400, 160 and 62 mm (Boespflug et al., 1995). According to the annual bed thickness, these cycles correspond to periods of 2, 5 and 12 years (Boespflug et al., 1995). Similarly, periods of 3, 5 and 15 years were determined from the bed thickness data (Boespflug et al., 1995). These periods are close to the periods identified in core 2220 glaciomarine sediments. This similarity suggests that both glaciomarine environments were influenced by a similar climatic forcing and that the NAO may have operated at similar periods during both the Holocene and Sangamonian. Furthermore, a sub-annual periodicity is also observed (17 mm) and likely corresponds to a seasonal cycle associated with the influence of alternating spring and neap tides on the sediments (Occhietti et al., 1995).

7. Conclusions

In this paper, we have shown that CAT-scan analysis of sedimentary sequences can be used to extract a continuous CT number profile with a pixel resolution of about 1 mm. This CT number profile reflects changes in bulk density, but is also affected by sediment consolidation. The long-term effect of sediment consolidation can be removed from the signal prior to spectral analysis. In examples from the St. Lawrence Estuary, spectral analysis of the CT number profiles of Holocene postglacial sediments revealed millennial- to centennial-scale oscillations possibly associated with either solar variability and changes in relative sea-level or tidal amplitude. Similarly, spectral analysis of the Holocene and Sangamonian glaciomarine sequences revealed decadal- to annual-scale oscillations with periods close to the ones previously associated with the NAO, whereas spectral analysis of the CT number profile of samples from the Sangamonian rhythmites possibly revealed seasonal cycles, illustrating the usefulness of this rapid and non-destructive method to study millennial to seasonal-scale climatic oscillations in sedimentary sequences. These sequences could either be terrestrial, lacustrine or marine.

Acknowledgments

We are in debt to the IPEV, Y. Balut, the captain, officers, crew and scientific participants of Leg 1 of the 1999 IMAGES-V cruise and to the X-ray department at the *Centre Hospitalier Régional de Rimouski* for access to the CAT-scan. This study was supported by a NSERC grant to Bernard F. Long and by a FQRNT postdoctoral fellowship to Guillaume St-Onge. Thanks are also due to Zoltan Hunyadfalvi and an anonymous reviewer for constructive comments. This is GEOTOP research centre contribution no. 2007-0054.

References

Aaby, B., 1976. Cyclic climatic variations in climate over the past 5,500 yr reflected in raised bogs. Nature 263, 281–284.
Amos, C.L., Sutherland, T.F., Radzijewski, B., Doucette, M., 1996. A rapid technique to determine bulk density of fine-grained sediments by X-ray computed tomography. Journal of Sedimentary Research 66, 1023–1039.
Appenzeller, C., Stocker, T.F., Anklin, M., 1998. North Atlantic Oscillation dynamics recorded in Greenland ice cores. Science 282, 446–449.
Boespflug, X., Long, B.F.N., Occhietti, S., 1995. CAT-scan in marine stratigraphy: a quantitative approach. Marine Geology 122, 281–301.
Cagnat, E., 2004. Étude sédimentologique de la série holocène de l'estuaire maritime du Saint-Laurent: apport de la tomodensitométrie. MSc Memoir. INRS-ETE, Québec, Canada.
Chapman, M.R., Shackleton, N.J., 2000. Evidence of 550-year and 1000-year cyclicities in North Atlantic circulation patterns during the Holocene. The Holocene 10, 287–291.
Cobb, K.M., Charles, C.D., Cheng, H., Edwards, R.L., 2003. El Niño/Southern Oscillation and tropical Pacific climate during the last millennium. Nature, 424, 271–276.
Cook, E.R., 2003. Multi-proxy reconstruction of the North Atlantic Oscillation (NAO) index: a critical review and a new well-verified winter NAO index reconstruction back to AD 1400. In: Hurrel, J.W., Kushnir, Y., Ottersen, G., Visbeck, M. (Eds.), The North Atlantic Oscillation Climatic Significance and Environmental Impact. Washington, DC. Geophysical Monograph, vol. 134. American Geophysical Union, pp. 63–79.
Crémer, J.-F., Long, B., Desrosiers, G., de Montety, L., Locat, J., 2002. Application de la scanographie à l'étude de la densité des sédiments et à la caractérisation des structures sédimentaires: exemple des sédiments déposés dans la rivière Saguenay (Québec, Canada) après la crue de juillet de 1996. Canadian Geotechnical Journal 39, 440–450.
D'Arrigo, R., Buckley, B., Kaplan, S., Woollett, J., 2003. Interannual to multidecadal modes of Labrador climate variability inferred from tree rings. Climate Dynamics 20, 219–228.
Fairbridge, R.W., Hillaire-Marcel, C., 1977. An 8,000-yr palaeoclimatic record of the 'Double-Hale' 45-yr solar cycle. Nature 268, 413–416.
Felis, T., Pätzold, J., Loya, Y., Fine, M., Nawar, A., Wefer, G., 2000. A coral oxygen isotope record from the northern Red Sea documenting NAO/ENSO, and North Pacific teleconnections on Middle East climate variability since the year 1750. Paleoceanography 15, 679–694.
Frisia, S., Borsato, A., Preto, N., McDermott, F., 2003. Late Holocene annual growth in three Alpine stalagmites records the influence of solar activity and the North Atlantic Oscillation on winter climate. Earth and Planetary Science Letters 216, 411–424.
Gray, S.T., Graumlich, L.J., Betancourt, J.L., Pederson, G.T., 2004. A tree-ring based reconstruction of the Atlantic Multidecadal Oscillation since 1567 A.D. Geophysical Research Letters 31. doi:10.1029/2004GL019932.
Holler, P., Kögler, F.C., 1990. Computer tomography: a nondestructive, high resolution technique for investigation of sedimentary structures. Marine Geology 91, 263–266.
Hu, F.S., Kaufman, D., Yoneji, S., Nelson, D., Shemesh, A., Huang, Y., Tian, J., Bond, G., Clegg, B., Brown, T., 2003. Cyclic variation and solar forcing of Holocene climate in the Alaskan subartic. Science 301, 1890–1893.
Hurrel, J.W., Kushnir, Y., Ottersen, G., Visbeck, M., 2003. An overview of the North Atlantic Oscillation. In: Hurrel, J.W., Kushnir, Y., Ottersen, G., Visbeck, M. (Eds.), The

North Atlantic Oscillation Climatic Significance and Environmental Impact. American Geophysical Union, Washington, DC, pp. 63–79.
Josenhans, H., Lehman, S., 1999. Late glacial stratigraphy and history of the Gulf of St. Lawrence, Canada. Canadian Journal of Earth Sciences 36, 1327–1345.
Kantzas, A., Marentette, D., Jha, K.N., 1992. Computer-assisted tomography: from qualitative visualization to quantitative core analysis. Journal of Petroleum Technology 31, 48–56.
Kunzendorf, H., Larsen, B., 2002. A 200–300 year cyclicity in sediment deposition in the Gotland Basin, Baltic Sea, as deduced from geochemical evidence. Applied Geochemistry 17, 29–38.
Lachniet, M., Burns, S., Piperno, D., Asmeron, Y., Polyak, V.J., Moy, C.M., Christenson, K., 2004. A 1500-year El Nino/Southern Oscillation and rainfall history for the Isthmus of Panama from speleothem calcite. Journal of Geophysical Research 109, D20117. doi:10.1029/2004JD004694.
Langdon, P.G., Barber, K.E., Hughes, P.D.M., 2003. A 7500-year peat-based palaeoclimatic reconstruction and evidence for a 1100-year cyclicity in bog surface wetness from Temple Hill Moss, Pentland Hills, southeast Scotland. Quaternary Science Reviews 22, 259–274.
Loring, D.H., Nota, D.J.G., 1973. Morphology and sediments of the Gulf of St. Lawrence. Bulletin of Fisheries Research Board of Canada 182, 147 pp.
Mermillod-Blondin, F., Marie, S., Desrosiers, G., Long, B., de Montety, L., Michaud, E., Stora, G., 2003. Assessment of the spatial variability of intertidal benthic communities by axial tomodensitometry: importance of fine-scale heterogeneity. Journal of Experimental Marine Biology and Ecology 287, 193–208.
Michaud, E., Desrosiers, G., Long, B., de Montety, L., Crémer, J.-F., Pelletier, E., Locat, J., Gilbert, F., Stora, G., 2003. Use of axial tomography to follow temporal changes of benthic communities in an unstable sedimentary environment (Baie des Ha!Ha!, Saguenay Fjord). Journal of Experimental Marine Biology and Ecology 285–286, 265–282.
Occhietti, S., Long, B., Clet, M., Boespflug, X., Sabeur, N., 1995. Séquence de la transition Illinoien–Sangamonien: forage IAC-91 de l'île aux Coudres, estuaire moyen du St-Laurent, Québec. Canadian Journal of Earth Sciences 32, 1950–1964.
Orsi, T.H., Edwards, C.M., Anderson, A.L., 1994. X-ray computed tomography: a non-destructive method for quantitative analysis of sediment cores. Journal of Sedimentary Research A64, 690–693.
Paillard, D., Labeyrie, L., Yiou, P., 1996. Macintosh program performs time-series analysis. Eos, Transactions, American Geophysical Union 77, 379.
Pepper, A.C., Shulmeister, J., Nobes, D.C., 2004. Possible ENSO signals prior to the Last Glacial maximum, during the last deglaciation and the early Holocene, from New Zealand. Geophysical Research Letters 31. doi:10.1029/2004GL020236.
Prasad, S., Heinz, V., Waldmann, N., Goldstein, S.L., Stein, M., 2004. Evidence from Lake Lisan of solar influence on decadal- to centennial-scale climate variability during marine oxygen isotope stage 2. Geology 32, 581–584.
Rampino, M.R., Sanders, J.E., 1981. Episodic growth of Holocene tidal marshes in the northeastern United States: a possible indicator of eustatic sea-level fluctuations. Geology 9, 63–67.
Schimmelmann, A., Lange, C., Meggers, B.J., 2003. Palaeoclimatic and archaeological evidence for a ~200-yr recurrence of floods and droughts linking California, Mesoamerica and South America over the past 2000 years. The Holocene 13, 763–778.
Schöne, B.N., Oschmann, W., Rössier, J., Freyre Castro, A.D., Houk, S.D., Krönke, I., Dreyer, W., Janssen, R., Rumohr, H., Dunca, E., 2004. North Atlantic dynamics recorded in shells of a long-lived bivalve mollusc. Geology 31, 1037–1040.
Shaw, J., Gareau, P., Courtney, R.C., 2002. Palaegeography of Atlantic Canada 13–0 kyr. Quaternary Science Reviews 21, 1861–1878.
Stenni, B., Jouzel, J., Masson-Delmotte, V., Röthlisberger, R., Castellano, E., Cattani, O., Falourd, S., Johnsen, S.J., Longinelli, A., Sachs, J.P., Selmo, E., Souchez, R., Steffensen, J.P., Udisti, R., 2003. A late-glacial high-resolution site and source temperature record derived from the EPICA Dome C isotope records (East Antarctica). Earth and Planetary Science Letters 217, 183–195.
St-Onge, G., 2004. Magnetic and sedimentological properties of Holocene sequences from the St. Lawrence Estuary and Saguenay Fjord, Canada. PhD thesis. Université du Québec à Montréal, Montréal, Canada.
St-Onge, G., Stoner, J.S., Hillaire-Marcel, C., 2003. Holocene paleomagnetic records from the St. Lawrence Estuary: centennial- to millennial-scale geomagnetic modulation of cosmogenic isotopes. Earth and Planetary Science Letters 209, 113–130.
Stuiver, M., Braziunas, T.F., 1993a. Modelling atmospheric ^{14}C influences and ^{14}C ages of marine samples to 10,000 BC. Radiocarbon 35, 137–189.
Stuiver, M., Braziunas, T.F., 1993b. Sun, ocean, climate and atmospheric $^{14}CO_2$: An evaluation of causal and spectral relationships. The Holocene 3, 189–305.
Stuiver, M., Grootes, P., Braziunas, T.F., 1995. The GISP2 $\delta^{18}O$ climate record of the past 16,500 years and the role of the sun, ocean and volcanoes. Quaternary Research 44, 341–354.
Syvitski, J.P.M., Praeg, D.B., 1989. Quaternary sedimentation in the St. Lawrence Estuary and adjoining areas, Eastern Canada: an overview based on high-resolution seismo-stratigraphy. Géographie Physique et Quaternaire 43, 291–310.
Tan, M., Hou, J., Liu, T., 2004. Sun-coupled climate connection between eastern Asia and northern Atlantic. Geophysical Research Letters 31, L07207. doi:10.1029/2004GL019085.
Vinther, B.M., Johnsen, S.J., Andersen, K.K., Clausen, H.B., Hansen, A.W., 2003. NAO signal recorded in the stable isotopes of Greenland ice cores. Geophysical Research Letters 30, 1387. doi:10.1029/2002GL016193.
Wellington, S.L., Vinegar, H.J., 1987. X-ray computerized tomography. Journal of Petroleum Technology 2, 1951–1954.
Yu, S.-Y., 2003. Centennial-scale cycles in middle Holocene sea level along the southeastern Swedish Baltic coast. GSA Bulletin 115, 1404–1409.
Yu, Z., Ito, E., 1999. Possible solar forcing of century-scale drought frequency in the northern Great Plains. Geology 27, 263–266.